Ukrainian Journal of Physical Optics
ISSUE 3
2026

DISPERSIVE OPTICAL SOLITON PERTURBATION WITH SCHRODINGER-HIROTA EQUATION BY LIE SYMMETRY

LAKHVEER KAUR [1], AHMED H. ARNOUS [2,3], MUHAMMAD AMIN S. MURAD [4] & ANJAN BISWAS [5,6,7,8,9*]

[1] Department of Mathematics, Jaypee Institute of Information Technology, Noida–201304, India
[2] Department of Mathematical Sciences, Saveetha School of Engineering, SIMATS Chennai–602105, Tamilnadu, India
[3] Jadara Research Center, Jadara University, Irbid 21110, Jordan.
[4] Department of Mathematics, College of Science, University of Duhok, Duhok, Iraq
[5] Department of Mathematics & Physics, Grambling State University, Grambling, LA 71245–2715, USA
[6] Department of Mathematics, Faculty of Science, Karadeniz Technical University, Trabzon–61080, Türkiye
[7] Department of Physics and Electronics, Khazar University, Baku AZ–1096, Azerbaijan
[8] Applied Science Research Center, Applied Science Private University, Amman—11937, Jordan
[9] Department of Mathematics and Applied Mathematics, Sefako Makgatho Health Sciences University, Medunsa–0204, South Africa
*Corresponding author: biswas.anjan@gmail.com

Received: 21.07.2026

Abstract. This study investigates traveling-wave solutions of a perturbed Schrödinger–Hirota equation that includes third-order dispersion, nonlinear dispersion, intermodal dispersion, self-steepening, and self-frequency-shift terms. The complex equation is decomposed into an equivalent real coupled system, and its Lie point symmetries are determined. A compatible linear combination of the translation and phase-rotation generators yields a traveling-wave reduction, subject to an explicit relation between the phase frequency and the symmetry coefficient. For the zero integration-constant branch, the reduced nonlinear ordinary differential equation is treated with a generalized auxiliary-equation method. Hyperbolic, exponential, and Jacobi-elliptic solution families are obtained under stated nondegeneracy, reality, and denominator conditions. Their limiting behaviors distinguish kink-type, dark-type, bright-type, singular, and nonlocalized profiles. Intensity plots illustrate representative propagation morphologies but are not used as evidence of stability.

Keywords: dispersion, Lie symmetry, cnoidal waves, Schrödinger–Hirota equation, optical solitons
UDC: 535.3
DOI: 10.3116/16091833/Ukr.J.Phys.Opt.2026.03238

1. Introduction

In optical fibers, the balance between chromatic dispersion and self-phase modulation supports pulse localization. For ultrashort pulses, third-order dispersion, nonlinear dispersion, self-steepening, and self-frequency-shift effects can modify this balance and motivate higher-order nonlinear Schrödinger-type models [1–10]. Eq. (1) is therefore treated here as a generalized perturbed Schrödinger–Hirota equation. Lie symmetry analysis does not derive this model from the nonlinear Schrödinger equation (NLSE); instead, it is applied to the already specified governing equation to identify invariant reductions. Because arbitrary perturbation coefficients generally destroy complete integrability, soliton radiation is not analyzed in the present work, and no inverse-scattering representation is assumed.

Recent studies on nonlinear Schrödinger-type optical models have further confirmed the importance of analytical schemes in constructing periodic waves, stochastic optical solitons, higher-order dispersive structures, and optical-fiber solitary waves [11-13]. These contributions support the continued relevance of exact solution methods for investigating nonlinear wave propagation in dispersive optical media.

Previous studies of Schrödinger–Hirota-type equations (SHE) have frequently used auxiliary equations or direct traveling-wave substitutions to construct exact waves. The novelty of the present work does not lie in the generalized auxiliary-equation method alone or merely in producing an additional catalog of closed-form expressions. Instead, the governing complex equation is first written as an equivalent real coupled system, and its admitted Lie point-symmetry algebra is determined. A compatible combination of the translation and phase-rotation generators then produces an invariant traveling-wave reduction. Compatibility of the reduced real and imaginary equations selects an explicit nondegenerate coefficient branch and yields a Duffing-type amplitude equation whose effective coefficients combine the higher-order perturbation parameters. The auxiliary equation is subsequently used to classify the admissible hyperbolic, exponential, and Jacobi-elliptic orbit families, including their reality conditions, singularity criteria, asymptotic states, and elliptic-to-hyperbolic limits. Thus, the principal contribution is the symmetry-derived reduction, the associated parameter compatibility, and the unified classification of the resulting traveling-wave structures for the perturbed Schrödinger–Hirota model.

2. Lie symmetry reduction

2.1. Governing model

The SHE is an important extension of the standard NLSE and enables the modeling of ultrashort pulse dynamics in nonlinear dispersive media more accurately when higher–order effects become significant, due to its ability to incorporate higher–order dispersive and nonlinear effects. In this study, SHE is therefore considered:

$$\begin{aligned} &iq_t + aq_{xx} + c\,|\,q\,|^2\,q + i(\gamma q_{xxx} + \sigma\,|\,q\,|^2\,q_x) \\ &= i\alpha q_x + i\lambda(|\,q\,|^2\,q)_x + i\nu(|\,q\,|^2)_x q, \end{aligned} \tag{1}$$

where $q = q(x,t)$ represents the complex envelope of the wave field, with x denoting the spatial propagation coordinate and t the temporal coordinate. The coefficient a represents the chromatic dispersion (CD), while c characterizes the cubic Kerr nonlinearity responsible for self–phase modulation. The higher–order dispersive contribution is described by the parameter γ, which accounts for third–order dispersion effects that become prominent for femtosecond pulses. The coefficient σ describes nonlinear dispersion. On the right–hand side, the term involving α corresponds to inter–modal dispersion. The coefficient λ represents self–steepening, which produces an intensity-dependent group delay, introduces temporal asymmetry, and can promote optical-shock-like edge formation in ultrashort pulses, while ν accounts for the soliton self–frequency shift.

Lie group analysis provides a systematic framework for determining continuous invariances, similarity variables, and reduced differential equations [14,15]. For the present higher-order optical model, the complex field is first decomposed into real and imaginary components. The resulting coupled system is then prolonged to third order, and the determining equations are solved to obtain the admitted translation and phase-rotation symmetries used below.

In this section, Lie symmetry analysis has been implemented for Eq. (1). As a preliminary step, the complex function $q(x,t)$ is decomposed into its real and imaginary components, expressed as

$$q(x,t)=u(x,t)+\imath v(x,t), \tag{2}$$

where $u(x,t)$ and $v(x,t)$ are real–valued functions. This representation facilitates transforming of the governing equation into an equivalent system of real partial differential equations, which is more convenient for carrying out this symmetry analysis. Then, Eq. (1) is rewritten as the following system of nonlinear equations for further analysis:

$$\begin{aligned} &-v_t+au_{xx}+c(u^2+v^2)u-\gamma v_{xxx}-\sigma(u^2+v^2)v_x=-\alpha v_x-\lambda\left((u^2+v^2)v\right)_x-\nu(u^2+v^2)_x v, \\ &u_t+av_{xx}+c(u^2+v^2)v+\gamma u_{xxx}+\sigma(u^2+v^2)u_x=\alpha u_x-\lambda\left((u^2+v^2)u\right)_x-\nu(u^2+v^2)_x u. \end{aligned} \tag{3}$$

Here, x and t denote the spatial propagation coordinate and the temporal coordinate, respectively, while $u(x,t)$ and $v(x,t)$ are the real and imaginary parts of the complex envelope $q(x,t)$. Subscripts indicate partial differentiation; for example, $u_t=\partial u/\partial t$, $u_{xx}=\partial^2 u/\partial x^2$, and $v_{xxx}=\partial^3 v/\partial x^3$. The quantity $u^2+v^2=|q|^2$ is the optical intensity. The real constants a, c, γ, σ, α, λ, and ν denote chromatic dispersion, Kerr nonlinearity, third-order dispersion, nonlinear dispersion, intermodal dispersion, self-steepening, and self-frequency shift, respectively. Parentheses followed by the subscript x, such as $\left((u^2+v^2)v\right)_x$, mean that the entire enclosed expression is differentiated with respect to x.

2.2. Symmetry structure of the real coupled syetem

Let us assume that the system of nonlinear partial differential Eq. (3), involving two dependent variables $u(x,t)$ and $v(x,t)$, is represented as

$$\begin{aligned} &\Delta_1(x,t,u,v,u_x,u_t,\ldots,u_{xxx},v_{xxx})=0, \\ &\Delta_2(x,t,u,v,u_x,u_t,\ldots,u_{xxx},v_{xxx})=0, \end{aligned} \tag{4}$$

Here, x and t denote the independent variables, and the system includes derivatives up to third order.

We introduce a one–parameter local Lie group of transformations acting on the variables x, t, $u(x,t)$, and $v(x,t)$ as

$$\begin{aligned} &x^*=x+\epsilon\xi^x(x,t,u,v)+O(\epsilon^2), \\ &t^*=t+\epsilon\xi^t(x,t,u,v)+O(\epsilon^2), \\ &u^*=u+\epsilon\eta^u(x,t,u,v)+O(\epsilon^2), \\ &v^*=v+\epsilon\eta^v(x,t,u,v)+O(\epsilon^2), \end{aligned} \tag{5}$$

where ϵ is a small parameter. The functions ξ^x, ξ^t, η^u, η^v represent the infinitesimal generators of the considered transformation, and the corresponding vector field is expressed as

$$\mathbf{X}=\xi^x\frac{\partial}{\partial x}+\xi^t\frac{\partial}{\partial t}+\eta^u\frac{\partial}{\partial u}+\eta^v\frac{\partial}{\partial v}. \tag{6}$$

Since the system involves derivatives up to third order, the symmetry generator must be prolonged accordingly to generate the invariance conditions. The third prolongation of $\mathbf{X}$ is written as

$$\mathrm{pr}^{(3)}\mathbf{X} = \mathbf{X} + \sum \eta^{u(J)} \frac{\partial}{\partial u_J} + \sum \eta^{v(J)} \frac{\partial}{\partial v_J} \tag{7}$$

where J denotes multi-indices corresponding to derivatives of order up to three. The associated coefficients with first-order derivatives are given by

$$\begin{aligned} \eta^u{}_x &= D_x(\eta^u) - u_x D_x(\xi^x) - u_t D_x(\xi^t), \\ \eta^u{}_t &= D_t(\eta^u) - u_x D_t(\xi^x) - u_t D_t(\xi^t), \\ \eta^v{}_x &= D_x(\eta^v) - v_x D_x(\xi^x) - v_t D_x(\xi^t), \\ \eta^v{}_t &= D_t(\eta^v) - v_x D_t(\xi^x) - v_t D_t(\xi^t). \end{aligned} \tag{8}$$

Higher-order terms are obtained recursively. For instance,

$$\begin{aligned} \eta^u{}_{xx} &= D_x(\eta^u{}_x) - u_{xx} D_x(\xi^x) - u_{xt} D_x(\xi^t), \\ \eta^u{}_{xxx} &= D_x(\eta^u{}_{xx}) - u_{xxx} D_x(\xi^x) - u_{xxt} D_x(\xi^t), \end{aligned} \tag{9}$$

and analogous expressions hold for η^v. The prolongation coefficients are computed using the total derivative operators such as

$$\begin{aligned} D_x &= \frac{\partial}{\partial x} + u_x \frac{\partial}{\partial u} + v_x \frac{\partial}{\partial v} + u_{xx} \frac{\partial}{\partial u_x} + v_{xx} \frac{\partial}{\partial v_x} + \cdots, \\ D_t &= \frac{\partial}{\partial t} + u_t \frac{\partial}{\partial u} + v_t \frac{\partial}{\partial v} + u_{xt} \frac{\partial}{\partial u_x} + v_{xt} \frac{\partial}{\partial v_x} + \cdots. \end{aligned} \tag{10}$$

The system is said to admit the symmetry generated by $\mathbf{X}$ if the prolonged vector field annihilates the system on its solution manifold, that is,

$$\begin{aligned} \mathrm{pr}^{(3)}\mathbf{X}(\Delta_1)|_{\Delta_1=0,\,\Delta_2=0} &= 0, \\ \mathrm{pr}^{(3)}\mathbf{X}(\Delta_2)|_{\Delta_1=0,\,\Delta_2=0} &= 0. \end{aligned} \tag{11}$$

Substitution of the prolonged expressions into the invariance conditions yields a system of linear partial differential equations for the infinitesimals $\xi^x(x,t,u,v)$, $\xi^t(x,t,u,v)$, $\eta^u(x,t,u,v)$, and $\eta^v(x,t,u,v)$. Solving this system provides the symmetry structure of the given PDE system. Using symbolic computation via Maple, the determining equations for the infinitesimals are solved systematically. As a result, the admitted infinitesimal generators are obtained as follows:

$$\xi^x = 0, \quad \xi^t = 1, \quad \eta^u = 0, \quad \eta^v = 0, \tag{12}$$

$$\xi^x = 1, \quad \xi^t = 0, \quad \eta^u = 0, \quad \eta^v = 0, \tag{13}$$

$$\xi^x = 0, \quad \xi^t = 0, \quad \eta^u = v, \quad \eta^v = -u. \tag{14}$$

These infinitesimals correspond to fundamental continuous symmetries of the governing system. In particular, they generate time translation, space translation, and phase rotation invariances, respectively. The associated Lie point symmetry generators can therefore be written in vector field form as

$$X_1 = \frac{\partial}{\partial t}, \tag{15}$$

$$X_2 = \frac{\partial}{\partial x}, \tag{16}$$

$$X_3 = v\frac{\partial}{\partial u} - u\frac{\partial}{\partial v}. \tag{17}$$

Here, X_1 and X_2 represent invariance under translations in time and space, while X_3 corresponds to rotational invariance in the (u,v)-plane, which is equivalent to the phase invariance of the complex function $q(x,t)$.

2.3. Lie algebra structure

To understand the underlying algebraic structure, the commutation relations between the symmetry generators are computed. A straightforward calculation yields

$$[X_1,X_2]=0,\ \ [X_1,X_3]=0,\ \ [X_2,X_3]=0. \tag{18}$$

This shows that all generators commute pairwise, and hence the symmetry algebra is Abelian. Consequently, the admitted Lie algebra is a three-dimensional Abelian Lie algebra given by

$$\mathfrak{g}=\langle X_1,X_2,X_3\rangle \cong \mathbb{R}^3. \tag{19}$$

Since the Lie algebra is Abelian, the adjoint action is trivial, i.e., the generators remain invariant under the adjoint representation. These generators provide inequivalent symmetry reductions of the governing system. In particular,

- The generator X_1 yields time-independent (stationary) solutions.
- The generator X_2 produces spatially invariant solutions.
- The generator X_3 corresponds to phase-invariant solutions, preserving the modulus of the complex field.

2.4. Similarity reduction

Next, we consider the following combined generator to produce invariant traveling-wave families for Eq. (1):

$$X=X_1+\Lambda X_2+\Omega X_3=\frac{\partial}{\partial t}+\Lambda\frac{\partial}{\partial x}+\Omega\left(v\frac{\partial}{\partial u}-u\frac{\partial}{\partial v}\right), \tag{20}$$

where Λ is the traveling velocity and Ω is the phase-rotation rate. Solving the corresponding characteristic equations,

$$\frac{dx}{\xi^x}=\frac{dt}{\xi^t}=\frac{du}{\eta^u}=\frac{dv}{\eta^v},$$

gives the similarity representation

$$\begin{aligned} q(x,t) &= p(\tau)\exp\big(i\phi(x,t)\big), \\ \phi(x,t) &= -k_1x+k_2t+k_3, \qquad \tau=x-\Lambda t, \end{aligned} \tag{21}$$

where p is the new dependent variable. The representation in Eq. (21) is invariant under the generator in Eq. (20) provided that

$$\Omega=\Lambda k_1-k_2. \tag{22}$$

This compatibility relation shows that the phase and traveling coordinate follow from the same symmetry action, rather than from an independently imposed traveling-wave ansatz. The similarity variables in (21) are substituted into Eq. (1). Then, the real and imaginary components are separated to obtain the following ordinary differential equations (ODEs):

$$(\lambda k_1-\sigma k_1-c)p(\tau)^3+\left(\gamma k_1^3+ak_1^2+\alpha k_1+k_2\right)p(\tau)+(-3\gamma k_1-a)p(\tau)_{\tau\tau}=0, \tag{23}$$

$$(3\gamma k_1^2+3p(\tau)^2\lambda+2p(\tau)^2\nu-p(\tau)^2\sigma+2ak_1+\Lambda+\alpha)p(\tau)_\tau-\gamma\, p(\tau)_{\tau\tau\tau}=0. \tag{24}$$

Eq. (23) yields the following parameter expressions for k_1, k_2, a :

$$k_1 = -\frac{1}{3}\frac{a}{\gamma}, \quad k_2 = \frac{1}{27}\frac{a\left(-2a^2+9\alpha\gamma\right)}{\gamma^2}, \quad a = -\frac{3c\gamma}{-\sigma+\lambda}. \tag{25}$$

The symmetry-compatible branch in Eq. (25) requires $\gamma \neq 0$ and $\lambda \neq \sigma$. The latter condition excludes the degenerate case in which the carrier wavenumber and the chromatic-dispersion compatibility relation become undefined. Substituting the parameter values in (25) into (24) leads to the following modified ODE:

$$\begin{aligned}&\left(3\lambda^3+2\lambda^2\nu-7\lambda^2\sigma-4\lambda\nu\sigma+5\lambda\sigma^2+2\nu\sigma^2-\sigma^3\right)p'(\tau)p(\tau)^2\\&+\left(-\gamma\lambda^2+2\gamma\lambda\sigma-\gamma\sigma^2\right)p'''(\tau)\\&+\left(\Lambda\lambda^2-2\Lambda\lambda\sigma+\Lambda\sigma^2+\alpha\lambda^2-2\alpha\lambda\sigma+\alpha\sigma^2-3c^2\gamma\right)p'(\tau)=0.\end{aligned} \tag{26}$$

Eq. (26) is integrated with respect to τ, and the reduced ODE is written as

$$\begin{aligned}&\frac{1}{3}\left(3\lambda^3+2\lambda^2\nu-7\lambda^2\sigma-4\lambda\nu\sigma+5\lambda\sigma^2+2\nu\sigma^2-\sigma^3\right)p(\tau)^3\\&+\left(-\gamma\lambda^2+2\gamma\lambda\sigma-\gamma\sigma^2\right)p''(\tau)\\&+\left(\Lambda\lambda^2-2\Lambda\lambda\sigma+\Lambda\sigma^2+\alpha\lambda^2-2\alpha\lambda\sigma+\alpha\sigma^2-3c^2\gamma\right)p(\tau)=0.\end{aligned} \tag{27}$$

The polynomial coefficients in Eq. (27) admit the factorizations

$$3\lambda^3+2\lambda^2\nu-7\lambda^2\sigma-4\lambda\nu\sigma+5\lambda\sigma^2+2\nu\sigma^2-\sigma^3=(\lambda-\sigma)^2\left(3\lambda+2\nu-\sigma\right),$$

and

$$-\gamma\lambda^2+2\gamma\lambda\sigma-\gamma\sigma^2=-\gamma(\lambda-\sigma)^2.$$

Consequently, Eq. (27) can be written in the compact form

$$-\gamma(\lambda-\sigma)^2p''+\frac{(\lambda-\sigma)^2\left(3\lambda+2\nu-\sigma\right)}{3}p^3+\left[\left(\Lambda+\alpha\right)(\lambda-\sigma)^2-3c^2\gamma\right]p=0. \tag{28}$$

For $\gamma \neq 0$ and $\lambda \neq \sigma$, division by $-\gamma(\lambda-\sigma)^2$ gives the Duffing-type amplitude equation

$$p''+\mu p+\beta p^3=0, \qquad \mu=\frac{3c^2}{(\lambda-\sigma)^2}-\frac{\Lambda+\alpha}{\gamma}, \qquad \beta=-\frac{3\lambda+2\nu-\sigma}{3\gamma}. \tag{29}$$

Its first integral is

$$\frac{1}{2}(p')^2+\frac{\mu}{2}p^2+\frac{\beta}{4}p^4=E, \tag{30}$$

where E is an integration constant. This representation shows that the higher-order perturbations do not act independently on the exact branch considered here. Their influence is organized through the combinations $\lambda-\sigma$, $3\lambda+2\nu-\sigma$, and $\Lambda+\alpha$. The first combination controls the carrier-wavenumber and dispersion compatibility, the second determines the effective cubic response, and the third represents the combined propagation and intermodal drift. The hyperbolic, exponential, and elliptic expressions derived below are therefore orbit families of the quartic effective potential in Eq. (30), rather than unrelated closed-form formulas.

For example, the zero-pedestal canonical bright branch, when $\mu<0$ and $\beta>0$, has the form

$$p(\tau)=\sqrt{\frac{2(-\mu)}{\beta}}\operatorname{sech}\left(\sqrt{-\mu}\,\tau\right), \tag{31}$$

so its peak intensity is $2(-\mu)/\beta$ and its characteristic width scales as $(-\mu)^{-1/2}$. When $\mu>0$ and $\beta<0$, the canonical kink branch is

$$p(\tau)=\sqrt{-\frac{\mu}{\beta}}\tanh\left(\sqrt{\frac{\mu}{2}}\tau\right), \tag{32}$$

with asymptotic intensity $-\mu/\beta$ and transition width proportional to $\sqrt{2/\mu}$. These expressions provide direct measures of how the perturbation parameters modify the amplitude and width while preserving the compatibility conditions.

Next, the generalized auxiliary equation approach is employed for the reduced nonlinear Eq. (27) to construct its exact solutions. This method is based on a systematic procedure that combines an appropriate functional transformation with a balancing principle that relates the highest–order derivative terms to the nonlinear components of the equation. By introducing a suitable ansatz, the governing equation is reduced to an auxiliary ordinary differential equation, which can be solved analytically. The strength of this methodology lies in its ability to generate a wide class of exact and closed–form solutions, including solitary-wave and periodic structures. In the subsequent analysis, this technique is used to derive exact solutions of Eq. (27), and a wide range of exact solutions is then obtained in a unified manner by reverting to the original spatial and temporal variables, with several free parameters.

By applying the homogeneous balancing principle to the higher–order linear and nonlinear terms in Eq. (27), the subsequent solution structure is formulated:

$$p(\tau)=T_0+\frac{T_1}{F(\tau)}+T_2F(\tau), \tag{33}$$

where $F(\tau)$ satisfies the following auxiliary equation:

$$F'(\tau)=\left(m_0+m_1F(\tau)+m_2F(\tau)^2+m_3F(\tau)^3+m_4F(\tau)^4\right)^{\frac{1}{2}}. \tag{34}$$

By substituting (33) into Eq. (27), together with its derivatives, as defined by Eq. (34), a polynomial expression in $F(\tau)$ is found. Collecting the coefficients corresponding to each power of $F(\tau)$ and setting them to zero yields a system of equations in the unknown parameters. Solving the resulting system of equations, the following categories are recovered to generate exact solutions of (27):

2.4.1. Category I. For the parameter values $m_1=\dfrac{m_3\left(4m_2m_4-m_3^2\right)}{8m_4^2}$, $m_0=\dfrac{\left(4m_2m_4-m_3^2\right)^2}{64m_4^3}$, the solution of the resulting algebraic system is obtained as follows:

Case 1.

$$\begin{gathered}\Lambda=\frac{Y_1}{8m_4\left(\lambda^2-2\lambda\sigma+\sigma^2\right)}, \quad T_0=\pm\frac{1}{4}\frac{\gamma m_3\sqrt{6}}{\sqrt{(2\nu-\sigma+3\lambda)\gamma m_4}}, \\ T_1=\pm\frac{1}{8}\frac{\left(4m_2m_4-m_3^2\right)\gamma\sqrt{6}}{\sqrt{(2\nu-\sigma+3\lambda)\gamma m_4}\,m_4}, \quad T_2=0,\end{gathered} \tag{35}$$

where

$$\begin{aligned}Y_1=&\,8\gamma\lambda^2m_2m_4-3\gamma\lambda^2m_3^2-16\gamma\lambda\sigma m_2m_4+6\gamma\lambda\sigma m_3^2+8\gamma\sigma^2m_2m_4\\&-3\gamma\sigma^2m_3^2-8\alpha\lambda^2m_4+16\alpha\lambda\sigma m_4-8\alpha\sigma^2m_4+24c^2\gamma m_4.\end{aligned}$$

Consequently, Eq. (27) has the following hyperbolic function solution, with $8m_2m_4 - 3m_3{}^2 \langle 0,\ \ m_4 \rangle 0$:

$$
\begin{aligned}
p_1(\tau) = {} & \pm\frac{(4m_2m_4 - m_3{}^2)\gamma\sqrt{6}}{8\sqrt{(2\nu-\sigma+3\lambda)\gamma m_4}\,m_4} \\
& \times\left(-\frac{m_3}{4m_4} + \frac{\sqrt{-8m_2m_4+3m_3{}^2}}{4m_4}\tanh\left(\frac{\sqrt{-m_4(8m_2m_4-3m_3{}^2)}\tau}{4m_4}\right)\right)^{-1} \\
& \pm\frac{\gamma m_3\sqrt{6}}{4\sqrt{(2\nu-\sigma+3\lambda)\gamma m_4}},
\end{aligned}
\tag{36}
$$

$$
\begin{aligned}
p_2(\tau) = {} & \pm\frac{(4m_2m_4 - m_3{}^2)\gamma\sqrt{6}}{8\sqrt{(2\nu-\sigma+3\lambda)\gamma m_4}\,m_4} \\
& \times\left(-\frac{m_3}{4m_4} + \frac{\sqrt{-8m_2m_4+3m_3{}^2}}{4m_4}\coth\left(\frac{\sqrt{-m_4(8m_2m_4-3m_3{}^2)}\tau}{4m_4}\right)\right)^{-1} \\
& \pm\frac{\gamma m_3\sqrt{6}}{4\sqrt{(2\nu-\sigma+3\lambda)\gamma m_4}},
\end{aligned}
\tag{37}
$$

The corresponding solutions of Eq. (1), written in the original variables x and t by using equation (21) together with Eqs. (36) and (37), are given by

$$
\begin{aligned}
q_1(x,t) = {} & p_1(x-\Lambda t) \\
& \times\exp\left(\iota\left(\frac{tc}{9\gamma(-\sigma+\lambda)}\left(-\frac{18c^2\gamma^2}{(-\sigma+\lambda)^2}+9\alpha\gamma\right)-\frac{xc}{-\sigma+\lambda}+k_3\right)\right),
\end{aligned}
\tag{38}
$$

$$
\begin{aligned}
q_2(x,t) = {} & p_2(x-\Lambda t) \\
& \times\exp\left(\iota\left(\frac{tc}{9\gamma(-\sigma+\lambda)}\left(-\frac{18c^2\gamma^2}{(-\sigma+\lambda)^2}+9\alpha\gamma\right)-\frac{xc}{-\sigma+\lambda}+k_3\right)\right)
\end{aligned}
\tag{39}
$$

The solution q_1 is a reciprocal tanh–type nonsingular kink soliton on a finite pedestal, provided that its denominator is nonzero. The solution q_2 is a reciprocal coth–type singular soliton because the coth factor generates a pole in the traveling-wave profile.

Case II.

$$
\begin{aligned}
& \Lambda = \frac{Y_1}{8m_4(\lambda^2 - 2\lambda\sigma + \sigma^2)}, \\
& T_0 = \pm\frac{1}{4}\frac{\gamma m_3\sqrt{6}}{\sqrt{(2\nu-\sigma+3\lambda)\gamma m_4}}, \\
& T_1 = 0,\ \ T_2 = \pm\frac{\sqrt{6}\sqrt{(2\nu-\sigma+3\lambda)\gamma m_4}}{2\nu-\sigma+3\lambda},
\end{aligned}
\tag{40}
$$

where

$$
\begin{aligned}
Y_1 = {} & 8\gamma\lambda^2 m_2m_4 - 3\gamma\lambda^2 m_3^2 - 16\gamma\lambda\sigma m_2m_4 + 6\gamma\lambda\sigma m_3^2 + 8\gamma\sigma^2 m_2m_4 \\
& -3\gamma\sigma^2 m_3^2 - 8\alpha\lambda^2 m_4 + 16\alpha\lambda\sigma m_4 - 8\alpha\sigma^2 m_4 + 24c^2\gamma m_4.
\end{aligned}
$$

Consequently, Eq. (27) has the following hyperbolic function solution, with $8m_2m_4 - 3m_3{}^2 \langle 0,\ \ m_4 \rangle 0$:

$$p_3(\tau)=\pm\frac{\sqrt{6}\sqrt{(2\nu-\sigma+3\lambda)\gamma m_4}}{2\nu-\sigma+3\lambda}\times\left(-\frac{m_3}{4m_4}+\frac{\sqrt{-8m_2m_4+3m_3{}^2}}{4m_4}\tanh\left(\frac{\sqrt{-m_4(8m_2m_4-3m_3{}^2)}\tau}{4m_4}\right)\right)\pm\frac{\gamma m_3\sqrt{6}}{4\sqrt{(2\nu-\sigma+3\lambda)\gamma m_4}},\tag{41}$$

$$p_4(\tau)=\pm\frac{\sqrt{6}\sqrt{(2\nu-\sigma+3\lambda)\gamma m_4}}{2\nu-\sigma+3\lambda}\times\left(-\frac{m_3}{4m_4}+\frac{\sqrt{-8m_2m_4+3m_3{}^2}}{4m_4}\coth\left(\frac{\sqrt{-m_4(8m_2m_4-3m_3{}^2)}\tau}{4m_4}\right)\right)\pm\frac{\gamma m_3\sqrt{6}}{4\sqrt{(2\nu-\sigma+3\lambda)\gamma m_4}},\tag{42}$$

The corresponding solutions of Eq. (1), written in the original variables x and t by using Eq. (21) together with Eqs. (41) and (42), are given by

$$q_3(x,t)=p_3(x-\Lambda t)\exp\left(\iota\left(\frac{tc}{9\gamma(-\sigma+\lambda)}\left(-\frac{18c^2\gamma^2}{(-\sigma+\lambda)^2}+9\alpha\gamma\right)-\frac{xc}{-\sigma+\lambda}+k_3\right)\right),\tag{43}$$

$$q_4(x,t)=p_4(x-\Lambda t)\exp\left(\iota\left(\frac{tc}{9\gamma(-\sigma+\lambda)}\left(-\frac{18c^2\gamma^2}{(-\sigma+\lambda)^2}+9\alpha\gamma\right)-\frac{xc}{-\sigma+\lambda}+k_3\right)\right)\tag{44}$$

Here q_3 is a tanh–type dark/kink soliton on a nonzero background because its amplitude approaches two finite limiting states as $\tau\to\pm\infty$. The solution q_4 is a coth–type singular soliton, since $\coth(\cdot)$ is unbounded at the wave center.

2.4.2. Category II. For the parameter values $m_1=\frac{m_3(4m_2m_4-m_3^2)}{8m_4^2}$, $m_0=\frac{m_3^2(16m_2m_4-5m_3^2)}{256m_4^3}$, the solution of the resulting algebraic system is obtained as follows:

Case 1.

$$\Lambda=\frac{Y_2}{8m_4(\lambda^2-2\lambda\sigma+\sigma^2)},\quad T_1=0,\quad T_0=\pm\frac{\gamma m_3\sqrt{6}}{\sqrt{16(3\lambda+2\nu-\sigma)\gamma m_4}},\quad T_2=\pm\frac{\sqrt{6}\sqrt{(3\lambda+2\nu-\sigma)\gamma m_4}}{3\lambda+2\nu-\sigma},\tag{45}$$

where

$$Y_2=8\gamma\lambda^2m_2m_4-3\gamma\lambda^2m_3^2-16\gamma\lambda\sigma m_2m_4+6\gamma\lambda\sigma m_3^2+8\gamma\sigma^2m_2m_4-3\gamma\sigma^2m_3^2-8\alpha\lambda^2m_4+16\alpha\lambda\sigma m_4-8\alpha\sigma^2m_4+24c^2\gamma m_4.$$

Consequently, Eq. (27) has the following hyperbolic function solution:

For $8m_2m_4-3m_3^2<0$ and $m_4<0$, we have

$$p_5(\tau)=\pm\frac{\sqrt{6}\sqrt{(3\lambda+2\nu-\sigma)\gamma m_4}}{3\lambda+2\nu-\sigma}\times\left(-\frac{1}{4}\frac{m_3}{m_4}+\frac{1}{4}\frac{\sqrt{-16m_2m_4+6m_3^2}}{m_4}sech\left(\frac{1}{4}\sqrt{2}\frac{\sqrt{m_4\left(8m_2m_4-3m_3^2\right)}}{m_4}\tau\right)\right)\pm\frac{\gamma m_3\sqrt{6}}{4\sqrt{(3\lambda+2\nu-\sigma)\gamma m_4}}. \quad (46)$$

For $8m_2m_4-3m_3^2>0$ and $m_4>0$, we have

$$p_6(\tau)=\pm\frac{\sqrt{6}\sqrt{(3\lambda+2\nu-\sigma)\gamma m_4}}{3\lambda+2\nu-\sigma}\times\left(-\frac{1}{4}\frac{m_3}{m_4}+\frac{1}{4}\frac{\sqrt{16m_2m_4-6m_3^2}}{m_4}csch\left(\frac{1}{4}\sqrt{2}\frac{\sqrt{m_4\left(8m_2m_4-3m_3^2\right)}}{m_4}\tau\right)\right)\pm\frac{\gamma m_3\sqrt{6}}{4\sqrt{(3\lambda+2\nu-\sigma)\gamma m_4}}. \quad (47)$$

The corresponding solutions of Eq. (1), written in the original variables x and t by using Eq. (21) together with Eqs. (46) and (47), are given by

$$q_5(x,t)=\left(T_2\left(-\frac{1}{4}\frac{m_3}{m_4}+\frac{1}{4}\frac{\sqrt{-16m_2m_4+6m_3^2}}{m_4}\mathrm{sech}\left(\frac{1}{4}\sqrt{2}\frac{\sqrt{m_4\left(8m_2m_4-3m_3^2\right)}}{m_4}\tau\right)\right)+T_0\right)\times\exp(\iota\phi(x,t)),$$
$$q_6(x,t)=\left(T_2\left(-\frac{1}{4}\frac{m_3}{m_4}+\frac{1}{4}\frac{\sqrt{16m_2m_4-6m_3^2}}{m_4}\mathrm{csch}\left(\frac{1}{4}\sqrt{2}\frac{\sqrt{m_4\left(8m_2m_4-3m_3^2\right)}}{m_4}\tau\right)\right)+T_0\right)\times\exp(\iota\phi(x,t)) \quad (48)$$

The solution q_5 is a sech–type bright soliton on a constant pedestal; for admissible parameters that remove the pedestal, it becomes a pure bright soliton. The solution q_6 is a csch–type singular soliton because $csch(\cdot)$ has a pole at the origin.

Here,

$$\phi(x,t)=\left(\left(\frac{tc}{9\gamma(-\sigma+\lambda)}\left(-\frac{18c^2\gamma^2}{(-\sigma+\lambda)^2}+9\alpha\gamma\right)-\frac{xc}{-\sigma+\lambda}+k_3\right)\right),$$
$$\tau=x-\frac{Y_2}{8m_4\left(\lambda^2-2\lambda\sigma+\sigma^2\right)}t.$$

2.4.3. Category III. For the parameter values $m_0=0,\ m_1=0,\ m_3=0$, the solution of the resulting algebraic system is obtained as follows:

$$\Lambda=\frac{\gamma\lambda^2m_2-2\gamma\lambda\sigma m_2+\gamma\sigma^2m_2-\alpha\lambda^2+2\alpha\lambda\sigma-\alpha\sigma^2+3c^2\gamma}{\lambda^2-2\lambda\sigma+\sigma^2},$$
$$T_0=0,\quad T_1=0,\quad T_2=\pm\frac{\sqrt{6}\sqrt{(3\lambda+2\nu-\sigma)\gamma m_4}}{3\lambda+2\nu-\sigma} \quad (49)$$

Consequently, Eq. (26) has the following solution structure:

$$p_7(\tau)=\frac{4\sqrt{6}\sqrt{\gamma}\sqrt{(3\lambda+2\nu-\sigma)m_4}m_2\mathrm{e}^{(\tau+C_1)\sqrt{m_2}}}{\left(-4m_2m_4\mathrm{e}^{2\tau\sqrt{m_2}}+\mathrm{e}^{2C_1\sqrt{m_2}}\right)(3\lambda+2\nu-\sigma)} \tag{50}$$

The corresponding solution of Eq. (1), written in the original variables x and t by using Eq. (21) together with Eqs. (49) and (50), is given by

$$q_7(x,t)=\left(\frac{4\sqrt{6}\sqrt{\gamma}\sqrt{(3\lambda+2\nu-\sigma)m_4}m_2\mathrm{e}^{(x-\Lambda t+C_1)\sqrt{m_2}}}{\left(-4m_2m_4\mathrm{e}^{2(x-\Lambda t)\sqrt{m_2}}+\mathrm{e}^{2C_1\sqrt{m_2}}\right)(3\lambda+2\nu-\sigma)}\right)\exp(\iota\phi(x,t)), \tag{51}$$

The exponential family q_7 gives a localized bright–type solitary wave when the denominator remains nonzero. If the denominator vanishes for an admissible parameter set, the same expression represents a singular soliton.

Here,

$$\phi(x,t)=\left(\left(\frac{tc}{9\gamma(-\sigma+\lambda)}\left(-\frac{18c^2\gamma^2}{(-\sigma+\lambda)^2}+9\alpha\gamma\right)-\frac{xc}{-\sigma+\lambda}+k_3\right)\right).$$

2.4.4. Categor IV. For the parameter values $m_1=\dfrac{m_3\left(4m_2m_4-m_3^2\right)}{8m_4^2}$, $m_0=0$, the solution of the resulting algebraic system is obtained as follows:

Case 1.

$$\begin{gathered}\Lambda=\frac{Y_3}{8m_4\left(\lambda^2-2\lambda\sigma+\sigma^2\right)},\\ T_0=\pm\frac{\gamma\sqrt{6}m_3}{4\sqrt{m_4(3\lambda+2\nu-\sigma)\gamma}},\ T_1=0,\ T_2=\pm\frac{m_4\gamma\sqrt{6}}{\sqrt{m_4(3\lambda+2\nu-\sigma)\gamma}},\end{gathered} \tag{52}$$

where

$$\begin{aligned}Y_3&=8\gamma\lambda^2m_2m_4-3\gamma\lambda^2m_3^2-16\gamma\lambda\sigma m_2m_4+6\gamma\lambda\sigma m_3^2+8\gamma\sigma^2m_2m_4\\&-3\gamma\sigma^2m_3^2-8\alpha\lambda^2m_4+16\alpha\lambda\sigma m_4-8\alpha\sigma^2m_4+24c^2\gamma m_4\end{aligned}.$$

Consequently, Eq. (1) has the following solution structures in terms of Jacobi elliptic functions: for the elliptic solutions below, the unity–modulus limits $\mathrm{sn}(u,m)\to\tanh u$, $\mathrm{sn}(u,m)\to\tanh u$, $\mathrm{cn}(u,m)\to\mathrm{sech}u$, $\mathrm{dn}(u,m)\to\mathrm{sech}u$, $\mathrm{ns}(u,m)\to\coth u$, $\mathrm{nc}(u,m)\to\cosh u$, $\mathrm{nc}(u,m)\to\cosh u$, are used as $m\to1$. In each case, $\tau=x-\Lambda t$ and the same phase factor $\exp(\iota\phi(x,t))$ is retained.

Subcase 1.1. If $m_4<0$ and $\left(4m_4m_2-m_3^2\right)>0$, then

$$\begin{aligned}q_8(x,t)&=\left(T_0+T_2\left(-\frac{m_3}{4m_4}+\frac{m_3}{4m_4}\mathrm{cn}\left(\frac{\sqrt{-m_4\left(4m_2m_4-m_3{}^2\right)}(x-\Lambda t)}{2m_4},\frac{m_3}{2\sqrt{4m_2m_4-m_3{}^2}}\right)\right)\right)\\&\quad\times\exp(\iota\phi(x,t)),\\ q_9(x,t)&=\left(T_0+T_2\left(-\frac{m_3}{4m_4}\pm\frac{m_3}{4m_4}\,\mathrm{dn}\left(\frac{m_3}{4\sqrt{-m_4}}(x-\Lambda t),\frac{2\sqrt{4m_4m_2-m_3^2}}{m_3}\right)\right)\right)\\&\quad\times\exp(\iota\phi(x,t)),\end{aligned} \tag{53}$$

As $m \to 1$, the identities $\mathrm{cn}(u,m) \to \mathrm{sech}u$ and $dn(u,m) \to \mathrm{sech}u$ give

$$\begin{aligned} q_8^{(1)}(x,t) &= \left[T_0 + T_2 \left(-\frac{m_3}{4m_4} + \frac{m_3}{4m_4} sech\left(\frac{\sqrt{-m_4\left(4m_2m_4 - m_3^2\right)}}{2m_4} \tau \right) \right) \right] \\ &\times \exp(\iota\phi(x,t)), \\ q_9^{(1)}(x,t) &== \left[T_0 + T_2 \left(-\frac{m_3}{4m_4} \pm \frac{m_3}{4m_4} sech\left(\frac{m_3}{4\sqrt{-m_4}} \tau \right) \right) \right] \\ &\times \exp(\iota\phi(x,t)). \end{aligned} \tag{54}$$

Thus q_8 and q_9 are cnoidal/dnoidal periodic waves, and their unity–modulus limits are bright–type solitons on a finite pedestal.

Subcase 1.2. If $m_4 < 0$, $\left(4m_4m_2 - m_3^2\right) < 0$, and $\left(16m_4m_2 - 5m_3^2\right) < 0$, then

$$\begin{aligned} q_{10}(x,t) &= \left(T_0 + T_2 \left(-\frac{m_3}{4m_4} \pm T_3 \,\mathrm{cn}\left(\frac{\sqrt{m_4\left(4m_4m_2 - m_3^2\right)}}{2m_4}(x - \Lambda t), \frac{\sqrt{\left(4m_4m_2 - m_3^2\right)\left(16m_4m_2 - 5m_3^2\right)}}{2\left(4m_4m_2 - m_3^2\right)} \right) \right) \right) \\ &\times \exp(\iota\phi(x,t)), \\ q_{11}(x,t) &= \left(T_0 + T_2 \left(-\frac{m_3}{4m_4} \pm T_3 \,\mathrm{dn}\left(\frac{\sqrt{m_4\left(16m_4m_2 - 5m_3^2\right)}}{4m_4}(x - \Lambda t), \frac{2\sqrt{\left(4m_4m_2 - m_3^2\right)\left(16m_4m_2 - 5m_3^2\right)}}{16m_4m_2 - 5m_3^2} \right) \right) \right) \\ &\times \exp(\iota\phi(x,t)), \end{aligned} \tag{55}$$

In the limit $m \to 1$, the solutions in this subcase reduce to

$$\begin{aligned} q_{10}^{(1)}(x,t) &= \left[T_0 + T_2 \left(-\frac{m_3}{4m_4} \pm T_3 \mathrm{sech}\left(\frac{\sqrt{m_4\left(4m_4m_2 - m_3^2\right)}}{2m_4} \tau \right) \right) \right] \\ &\times \exp(\iota\phi(x,t)), \\ q_{11}^{(1)}(x,t) &= \left[T_0 + T_2 \left(-\frac{m_3}{4m_4} \pm T_3 \mathrm{sech}\left(\frac{\sqrt{m_4\left(16m_4m_2 - 5m_3^2\right)}}{4m_4} \tau \right) \right) \right] \\ &\times \exp(\iota\phi(x,t)). \end{aligned} \tag{56}$$

Therefore, q_{10} and q_{11} are elliptic periodic waves whose unity–modulus limits are bright–type solitons on a pedestal.

Here,

$$T_3 = \frac{\sqrt{-\left(16m_4m_2 - 5m_3^2\right)}}{4m_4}.$$

Subcase 1.3. If $m_4 < 0$, $\left(4m_4m_2 - m_3^2\right) > 0$, and $\left(16m_4m_2 - 5m_3^2\right) < 0$, then

$$q_{12}(x,t)=\left(T_0+T_2\left(\begin{array}{l}-\dfrac{m_3}{4m_4}\pm\dfrac{\sqrt{-\left(16m_4m_2-5m_3^2\right)}}{4m_4}\\ \times\mathrm{nc}\left(\dfrac{\sqrt{-m_4\left(4m_4m_2-m_3^2\right)}}{2m_4}(x-\Lambda t),\ \dfrac{m_3}{2\sqrt{4m_4m_2-m_3^2}}\right)\end{array}\right)\right)$$
$$\times\exp(\iota\phi(x,t)),$$
$$q_{13}(x,t)=\left(T_0+T_2\left(\begin{array}{l}-\dfrac{m_3}{4m_4}\pm\dfrac{\sqrt{-\left(16m_4m_2-5m_3^2\right)}}{4m_4}\\ \times\mathrm{nd}\left(\dfrac{m_3}{4\sqrt{-m_4}}(x-\Lambda t),\ \dfrac{2\sqrt{4m_4m_2-m_3^2}}{m_3}\right)\end{array}\right)\right)$$
$$\times\exp(\iota\phi(x,t)), \tag{57}$$

Since $\mathrm{nc}(u,m)\to\cosh u$ and $\mathrm{nd}(u,m)\to\cosh u$ as $m\to 1$, this subcase gives

$$q_{12}^{(1)}(x,t)=\left[T_0+T_2\left(-\frac{m_3}{4m_4}\pm\frac{\sqrt{-\left(16m_4m_2-5m_3^2\right)}}{4m_4}\cosh\left(\frac{\sqrt{-m_4\left(4m_4m_2-m_3^2\right)}}{2m_4}\tau\right)\right)\right]$$
$$\times\exp(\iota\phi(x,t)),$$
$$q_{13}^{(1)}(x,t)=\left[T_0+T_2\left(-\frac{m_3}{4m_4}\pm\frac{\sqrt{-\left(16m_4m_2-5m_3^2\right)}}{4m_4}\cosh\left(\frac{m_3}{4\sqrt{-m_4}}\tau\right)\right)\right]$$
$$\times\exp(\iota\phi(x,t)). \tag{58}$$

Thus q_{12} and q_{13} are reciprocal elliptic waves, and the hyperbolic $\cosh$ growth makes their unity–modulus limits nonlocalized singular-type profiles.

Subcase 1.4. If $\left(4m_4m_2-m_3^2\right)>0$ and $\left(4m_4m_2-m_3^2\right)\left(16m_4m_2-5m_3^2\right)>0$, then

$$q_{14}(x,t)=\left(T_0+T_2\left(-\frac{m_3}{4m_4}\pm\frac{m_3}{4m_4}\mathrm{nc}\left(\begin{array}{c}\dfrac{\sqrt{m_4\left(4m_4m_2-m_3^2\right)}}{2m_4}(x-\Lambda t),\\ \dfrac{\sqrt{\left(4m_4m_2-m_3^2\right)\left(16m_4m_2-5m_3^2\right)}}{2\left(4m_4m_2-m_3^2\right)}\end{array}\right)\right)\right)\exp(\iota\phi(x,t)),$$
$$q_{15}(x,t)=\left(T_0+T_2\left(-\frac{m_3}{4m_4}\pm\frac{m_3}{4m_4}\mathrm{nd}\left(\begin{array}{c}\dfrac{\sqrt{m_4\left(16m_4m_2-5m_3^2\right)}}{4m_4}(x-\Lambda t),\\ \dfrac{2\sqrt{\left(4m_4m_2-m_3^2\right)\left(16m_4m_2-5m_3^2\right)}}{16m_4m_2-5m_3^2}\end{array}\right)\right)\right)\exp(\iota\phi(x,t)), \tag{59}$$

Using the same reciprocal limits, $nc(u,m)\to\cosh u$ and $nd(u,m)\to\cosh u$, one obtains

$$q_{14}^{(1)}(x,t)==\left[T_0+T_2\left(-\frac{m_3}{4m_4}\pm\frac{m_3}{4m_4}\cosh\left(\frac{\sqrt{m_4\left(4m_4m_2-m_3^2\right)}}{2m_4}\tau\right)\right)\right]\exp(\iota\phi(x,t)),$$
$$q_{15}^{(1)}(x,t)=\left[T_0+T_2\left(-\frac{m_3}{4m_4}\pm\frac{m_3}{4m_4}\cosh\left(\frac{\sqrt{m_4\left(16m_4m_2-5m_3^2\right)}}{4m_4}\tau\right)\right)\right]\exp(\iota\phi(x,t)). \tag{60}$$

Accordingly, q_{14} and q_{15} are reciprocal elliptic periodic waves, while their unity–modulus limits are unbounded singular-type profiles.

Subcase–1.5. If $m_4>0$ and $\left(16m_4m_2-5m_3^2\right)<0$, then

$$q_{16}(x,t)=\left(T_0+T_2\left(-\frac{m_3}{4m_4}\pm\frac{m_3}{4m_4}\mathrm{nc}\left(\begin{array}{l}-\frac{m_3}{4m_4}\pm\frac{m_3}{4m_4}\\ \times\mathrm{ns}\left(\frac{m_3}{4\sqrt{m_4}}(x-\Lambda t),\frac{\sqrt{-\left(16m_4m_2-5m_3^2\right)}}{m_3}\right)\end{array}\right)\right)\right)$$
$$\times\exp(\iota\phi(x,t)),$$

$$q_{17}(x,t)=\left(T_0+T_2\left(\begin{array}{l}-\frac{m_3}{4m_4}\pm\frac{\sqrt{-\left(16m_4m_2-5m_3^2\right)}}{4m_4}\\ \times\mathrm{ns}\left(\frac{\sqrt{-m_4\left(16m_4m_2-5m_3^2\right)}}{4m_4}(x-\Lambda t),\frac{m_3}{\sqrt{-\left(16m_4m_2-5m_3^2\right)}}\right)\end{array}\right)\right)$$
$$\times\exp(\iota\phi(x,t)),\tag{61}$$

$$q_{18}(x,t)=\left(T_0+T_2\left(\begin{array}{l}-\frac{m_3}{4m_4}\pm\frac{\sqrt{-\left(16m_4m_2-5m_3^2\right)}}{4m_4}\\ \times\mathrm{sn}\left(\frac{m_3}{4\sqrt{m_4}}(x-\Lambda t),\frac{\sqrt{-\left(16m_4m_2-5m_3^2\right)}}{m_3}\right)\end{array}\right)\right)\exp(\iota\phi(x,t)),$$

$$q_{19}(x,t)=\left(T_0+T_2\left(\begin{array}{l}-\frac{m_3}{4m_4}\pm\frac{m_3}{4m_4}\\ \times\mathrm{sn}\left(\frac{\sqrt{-m_4\left(16m_4m_2-5m_3^2\right)}}{4m_4}(x-\Lambda t),\frac{m_3}{\sqrt{-\left(16m_4m_2-5m_3^2\right)}}\right)\end{array}\right)\right)$$
$$\times\exp(\iota\phi(x,t)),$$

For this last elliptic set, $\mathrm{nc}(u,m)\to\cosh u$, $\mathrm{ns}(u,m)\to\coth u$, and $\mathrm{sn}(u,m)\to\tanh u$ yield

$$q_{16}^{(1)}(x,t)=\left[T_0+T_2\left(-\frac{m_3}{4m_4}\pm\frac{m_3}{4m_4}\cosh\left(-\frac{m_3}{4m_4}\pm\frac{m_3}{4m_4}\coth\left(\frac{m_3}{4\sqrt{m_4}}\tau\right)\right)\right)\right]\exp(\iota\phi(x,t)),$$

$$q_{17}^{(1)}(x,t)=\left[T_0+T_2\left(-\frac{m_3}{4m_4}\pm\frac{\sqrt{-\left(16m_4m_2-5m_3^2\right)}}{4m_4}\coth\left(\frac{\sqrt{-m_4\left(16m_4m_2-5m_3^2\right)}}{4m_4}\tau\right)\right)\right]$$
$$\times\exp(\iota\phi(x,t)),\tag{62}$$

$$q_{18}^{(1)}(x,t)=\left[T_0+T_2\left(-\frac{m_3}{4m_4}\pm\frac{\sqrt{-\left(16m_4m_2-5m_3^2\right)}}{4m_4}\tanh\left(\frac{m_3}{4\sqrt{m_4}}\tau\right)\right)\right]\exp(\iota\phi(x,t)),$$

$$q_{19}^{(1)}(x,t)=\left[T_0+T_2\left(-\frac{m_3}{4m_4}\pm\frac{m_3}{4m_4}\tanh\left(\frac{\sqrt{-m_4\left(16m_4m_2-5m_3^2\right)}}{4m_4}\tau\right)\right)\right]\exp(\iota\phi(x,t)).$$

Consequently, q_{16} is a reciprocal elliptic family with a nonlocalized singular limiting profile, q_{17} is a reciprocal–snoidal family whose limit is a coth–type singular soliton, and q_{18} and q_{19}

are snoidal families whose limits are tanh–type dark/kink solitons on a nonzero background.

Here, $\phi(x,t)=\left(\left(\frac{tc}{9\gamma(-\sigma+\lambda)}\left(-\frac{18c^2\gamma^2}{(-\sigma+\lambda)^2}+9\alpha\gamma\right)-\frac{xc}{-\sigma+\lambda}+k_3\right)\right)$ in all the above subcases.

3. Results and discussion

This section presents the graphical interpretation of the recovered families of dispersive optical solitons. Since the exact solutions are complex-valued wave fields with a traveling-wave amplitude and a phase factor, the physically relevant measurable quantity is the intensity $|q(x,t)|^2$. The exponential phase factor has unit modulus; therefore, it does not affect the intensity distribution. Consequently, the graphical profiles shown in Figs. 1–6 represent the propagation behavior of the corresponding amplitude functions along the traveling coordinate $x-\Lambda t$. Figs. 1–6 display the intensity evolution of the selected solutions q_1,q_3,q_5,q_7,q_8, and q_9. For each solution, three complementary views are provided. The first panel shows the three-dimensional profile of $|q_j(x,t)|^2$, illustrating the overall spatiotemporal propagation pattern. The second panel gives the contour representation, which clarifies the localization, trajectory, and width of the wave structure in the (x,t)-plane. The third panel presents two-dimensional intensity cuts at different fixed times, showing how the profile is translated during propagation while preserving its qualitative structure.

Fig. 1 corresponds to the solution $q_1(x,t)$, which is generated from a reciprocal tanh–type amplitude. The intensity profile exhibits kink-type behavior on a finite background. The transition between the two asymptotic intensity levels is clearly visible in both the three-dimensional and two-dimensional plots. This confirms that q_1 does not represent a localized bright pulse, but rather a dark/kink-type structure whose intensity connects finite limiting states as $x-\Lambda t\to\pm\infty$.

Fig. 2 shows the behavior of the tanh–type solution $q_3(x,t)$. Similar to q_1, this solution describes a dark/kink optical soliton on a nonzero background. The two-dimensional cuts demonstrate that the transition region shifts with time without changing its essential shape. This behavior is consistent with the traveling-wave reduction, in which the wave motion is governed by the single variable $x-\Lambda t$. The contour plot further confirms the oblique propagation of the intensity front along the traveling direction.

Figs. 3 and 4 represent the localized bright–type structures associated with $q_5(x,t)$ and $q_7(x,t)$, respectively. The solution q_5 originates from a sech–type amplitude and therefore produces a localized peak in the intensity distribution. The maximum intensity remains concentrated around the wave center and moves along the characteristic line $x=\Lambda t+\text{constant}$. The exponential family q_7 also gives a localized solitary-wave structure for admissible parameter values that keep the denominator nonzero. The corresponding plots show a well-defined propagating peak.

Figs. 5 and 6 correspond to the elliptic-function solutions $q_8(x,t)$ and $q_9(x,t)$. These solutions are originally expressed in terms of cnoidal and dnoidal waves. In the unity–modulus limit, the Jacobi elliptic functions reduce to hyperbolic functions, and the resulting profiles become bright–type localized structures on a finite pedestal. The graphical results show localized intensity peaks superimposed on a nonzero background, which is consistent with the analytical reduction of the cnoidal and dnoidal solutions to their hyperbolic soliton limits.

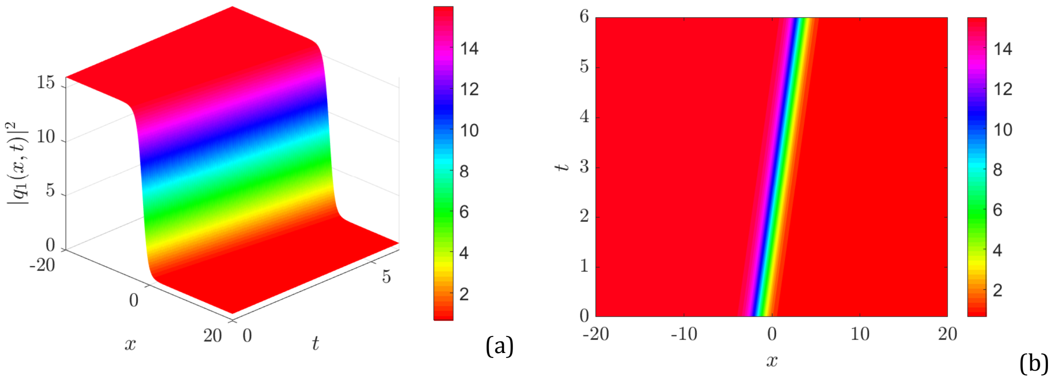

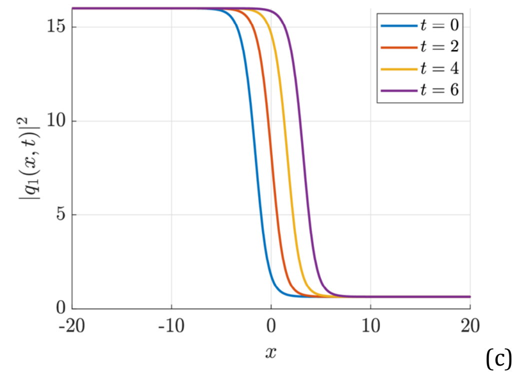

Fig. 1. Graphical representation of the intensity dynamics of the reciprocal tanh–type kink soliton solution $q_1(x,t)$. (a) Three-dimensional intensity profile of the reciprocal tanh–type kink soliton $|q_1(x,t)|^2$. (b) Contour plot of the intensity distribution$|q_1(x,t)|^2$. (c) Two-dimensional intensity profiles of $|q_1(x,t)|^2$at different times.

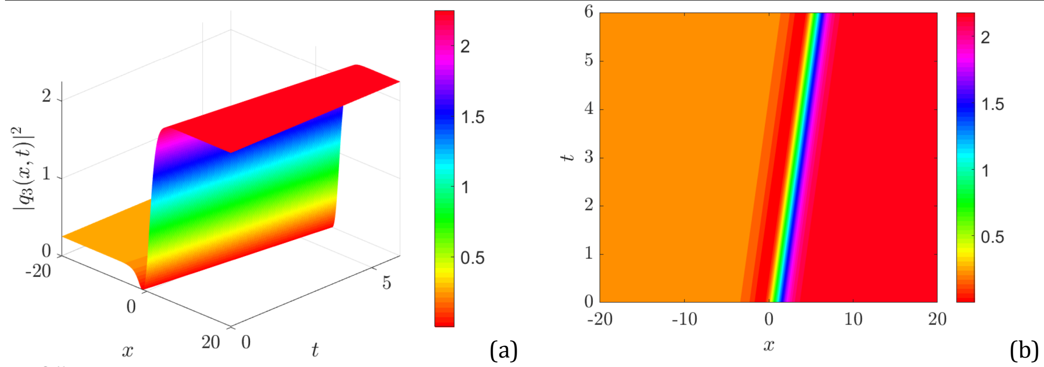

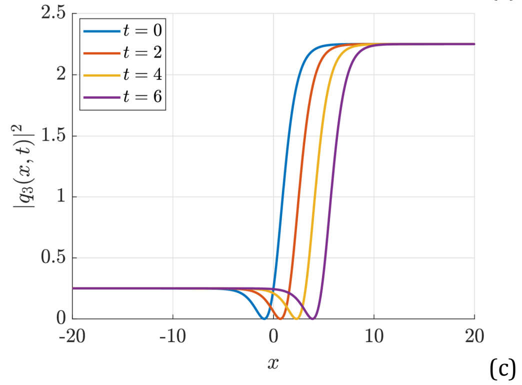

Fig. 2. Graphical representation of the intensity dynamics of the tanh–type dark/kink soliton solution $q_3(x,t)$. (a) Three-dimensional intensity profile of the tanh–type dark/kink soliton $|q_3(x,t)|^2$. (b) Contour plot of the intensity distribution $|q_3(x,t)|^2$. (c) Two-dimensional intensity profiles of $|q_3(x,t)|^2$ at different times.

The graphical results confirm the analytical classification of the recovered solutions. The profiles q_1 and q_3 display dark/kink-type behavior with finite background states, whereas q_5, q_7, q_8, and q_9 show localized bright–type propagation under the selected parameter settings.

These plots also demonstrate that the obtained solutions preserve their shapes during propagation, which is a characteristic feature of soliton dynamics. Thus, the graphical analysis supports the validity of the recovered exact solutions and highlights the role of the traveling-wave coordinate in controlling the motion of the dispersive optical structures.

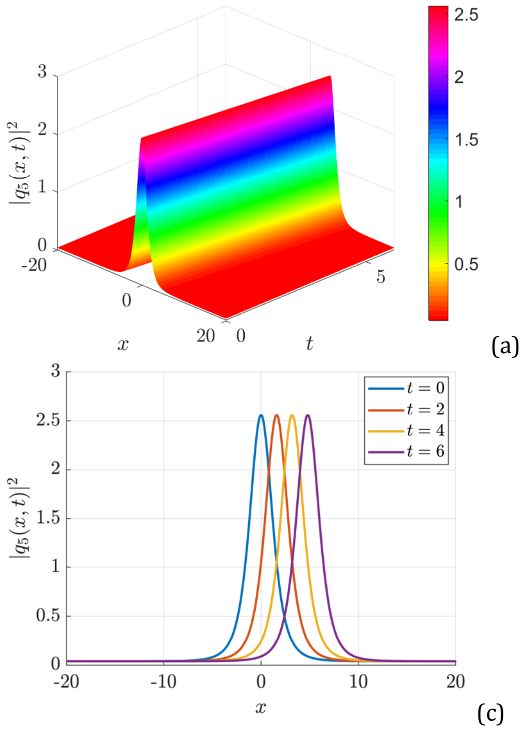

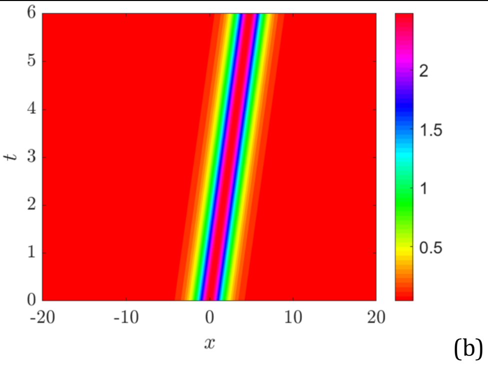

Fig. 3. Graphical representation of the intensity dynamics of the sech–type bright soliton solution $q_5(x,t)$. (a) Three-dimensional intensity profile of the sech–type bright soliton $|q_5(x,t)|^2$. (b) Contour plot of the intensity distribution $|q_5(x,t)|^2$. (c) Two-dimensional intensity profiles of $|q_5(x,t)|^2$ at different times.

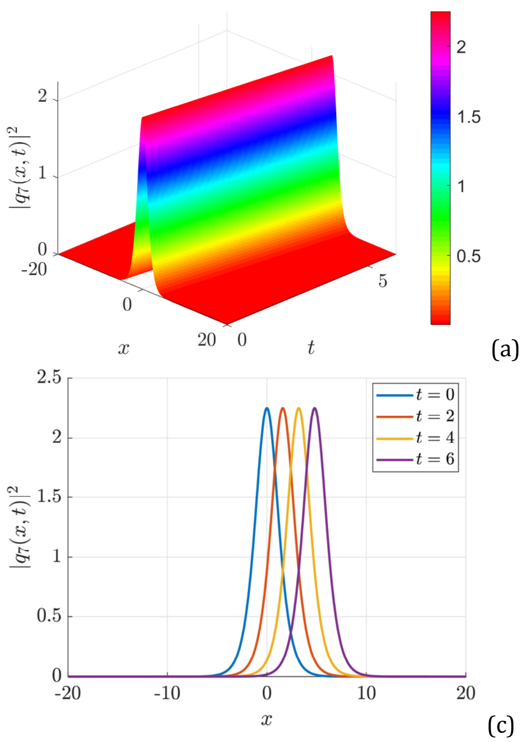

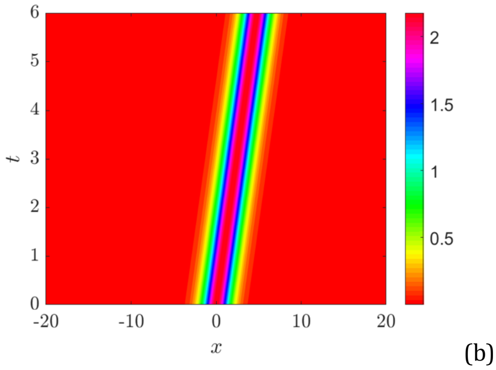

Fig. 4. Graphical representation of the intensity dynamics of the exponential localized soliton solution$q_7(x,t)$. (a) Three-dimensional intensity profile of the exponential localized soliton $|q_7(x,t)|^2$. (b) Contour plot of the intensity distribution $|q_7(x,t)|^2$. (c) Two-dimensional intensity profiles of $|q_7(x,t)|^2$ at different times.

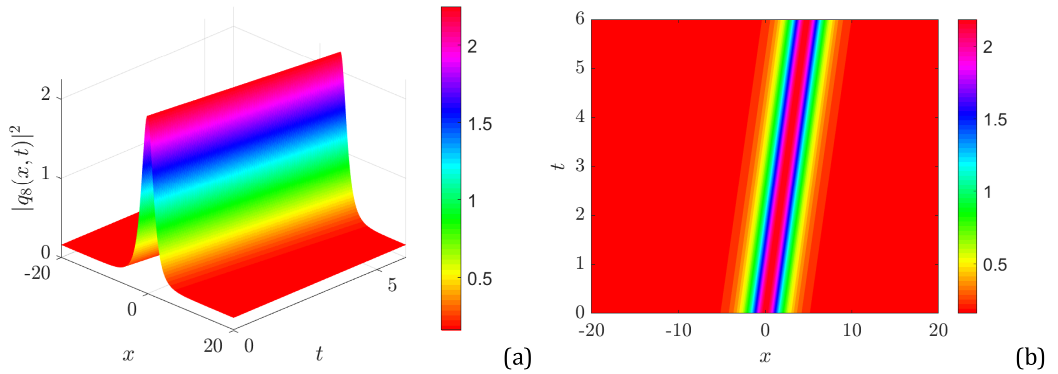

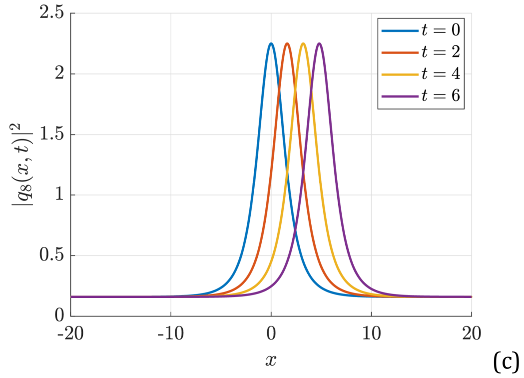

Fig. 5. Graphical representation of the intensity dynamics of the cnoidal wave solution $q_8(x,t)$ in its unity–modulus bright–type soliton limit. (a) Three-dimensional intensity profile of the cnoidal bright–type soliton limit $|q_8(x,t)|^2$. (b) Contour plot of the intensity distribution $|q_8(x,t)|^2$. (c) Two-dimensional intensity profiles of $|q_8(x,t)|^2$ at different times.

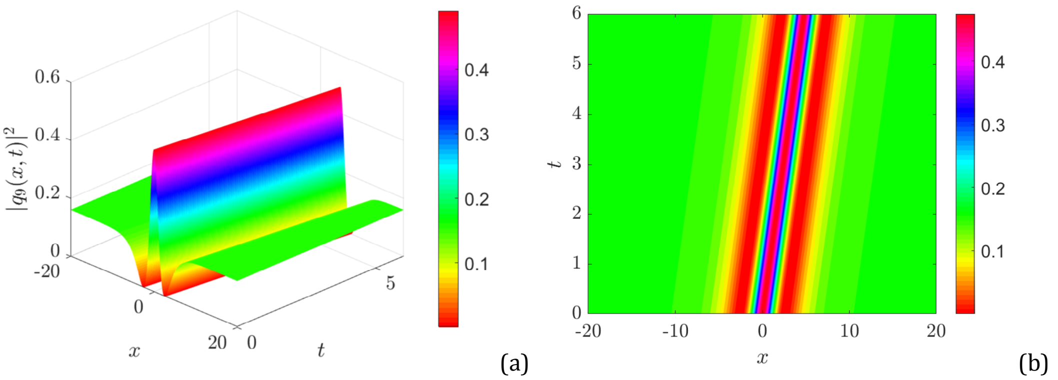

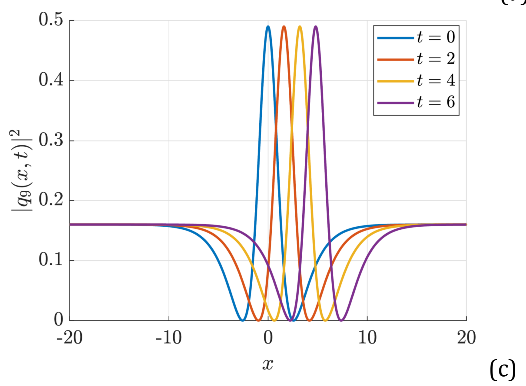

Fig. 6. Graphical representation of the intensity dynamics of the dnoidal wave solution $q_9(x,t)$ in its unity–modulus bright–type soliton limit. (a) Three-dimensional intensity profile of the dnoidal bright–type soliton limit $|q_9(x,t)|^2$. (b) Contour plot of the intensity distribution $|q_9(x,t)|^2$. (c) Two-dimensional intensity profiles of $|q_9(x,t)|^2$ at different times.

The third-order-dispersion coefficient γ determines the dispersive-curvature scale in the reduced amplitude equation. It appears in both effective coefficients μ and β, so changing its magnitude or sign modifies the balance among profile curvature, the linear restoring contribution, and nonlinear self-action. Consequently, γ affects the admissible amplitude and localization scale and may change the sign conditions required for bright, dark, kink, or periodic structures. This dependence is branch-specific and need not be monotonic because γ also enters the coefficient compatibility relation (Table 1).

The nonlinear-dispersion coefficient σ acts jointly with the self-steepening coefficient λ. Their difference $\lambda-\sigma$ determines the carrier wavenumber and enters the effective linear coefficient through $(\lambda-\sigma)^{-2}$. Thus, the limit $\lambda\to\sigma$ is singular for the selected reduction and must be excluded (Table 1). The combination $3\lambda+2\nu-\sigma$ controls the effective cubic response. Variations in σ can therefore modify the peak and background intensities, width, and existence conditions, and may shift the solution between bounded and singular parameter regimes.

The intermodal-dispersion coefficient α enters the reduced equation through $\Lambda+\alpha$. It therefore acts primarily as a drift or velocity correction. For fixed Λ, a change in α modifies μ and hence the profile amplitude and width. Alternatively, Λ may be adjusted to compensate for α, thereby allowing the intrinsic shape to remain unchanged while shifting the pulse trajectory in the (x,t) -plane. The coefficient α also contributes to the temporal phase frequency through Eq. (25) (Table 1).

The self-steepening coefficient λ represents an intensity-dependent group-velocity correction (Table 1). In general ultrashort-pulse propagation, self-steepening produces temporal asymmetry and can promote optical-shock-like edge formation. Within the invariant exact branch considered here, this effect is projected onto the combinations $\lambda-\sigma$ and $3\lambda+2\nu-\sigma$. It consequently changes the admissible amplitude, pedestal, propagation speed, and coefficient constraints. Because the present solutions are shape-preserving traveling waves, they do not reproduce the full transient development of an optical shock.

The self-frequency-shift coefficient ν enters the amplitude equation through $3\lambda+2\nu-\sigma$. Changing ν therefore modifies the effective cubic coefficient β, which controls the nonlinear contribution to the peak or background intensity and may alter the reality conditions of the exact solutions. Since the present ansatz contains a fixed linear carrier phase, these solutions do not describe a continuously evolving spectral displacement. Instead, the self-frequency-shift term influences the stationary traveling-wave balance and the associated admissible profile parameters (Table 1).

Table 1. Dependence of the symmetry-reduced wave profiles on the higher-order perturbation coefficients.

Coefficient	Appearance in the reduced branch	Principal influence on the wave profile
γ	μ, β, and the curvature term	Dispersive scale, width, amplitude, and the sign conditions for bounded branches.
σ	$\lambda-\sigma$ and $3\lambda+2\nu-\sigma$	Nonlinear dispersion, carrier wavenumber, effective cubic response, and degeneracy at $\sigma=\lambda$.
α	$\Lambda+\alpha$ and the temporal phase	Drift velocity, pulse trajectory, phase frequency, and, for fixed Λ, amplitude and width.
λ	$\lambda-\sigma$ and $3\lambda+2\nu-\sigma$	Self-steepening contribution, pedestal, amplitude, propagation speed, and existence conditions.
ν	$3\lambda+2\nu-\sigma$	Effective cubic response, peak or background intensity, and branch reality conditions.

The figures should be interpreted as illustrations of exact translation along $\tau = x - \Lambda t$, not as evidence of dynamical or spectral stability. The slope of each ridge or transition front in the (x,t)-plane is governed by Λ. The peak intensity, nonzero pedestal, and transition steepness are controlled by μ and β, and hence by the effective parameter combinations identified above. Bright profiles correspond to localized orbits of the quartic effective potential, dark and kink profiles connect finite-amplitude asymptotic states, and Jacobi-elliptic profiles represent periodic orbits whose modulus-one limits approach hyperbolic solitary waves. Singular profiles arise when the complete amplitude expression develops a pole at a finite value of the traveling coordinate. Any parameter-sensitivity comparison must preserve the compatibility condition in Eq. (25) and the reality conditions of the selected family; varying one coefficient while leaving an incompatible parameter set unchanged would not represent a solution of the governing equation.

4. Conclusions

This study derived symmetry-invariant traveling-wave solutions for a generalized perturbed Schrödinger–Hirota equation containing third-order dispersion, nonlinear dispersion, intermodal drift, self-steepening, and self-frequency-shift terms. The equivalent real system admits time translation, space translation, and phase rotation, which form a three-dimensional Abelian Lie algebra. A compatible combination of these generators produces the traveling coordinate and phase relation, while consistency of the reduced real and imaginary equations selects a nondegenerate coefficient branch.

On this branch, the amplitude equation reduces to a Duffing-type oscillator with a quartic first integral. Its effective linear and cubic coefficients depend on the combinations $\lambda - \sigma$, $3\lambda + 2\nu - \sigma$, and $\Lambda + \alpha$. This representation clarifies how the higher-order perturbations control the profile amplitude, background level, width, propagation velocity, and admissibility. The generalized auxiliary-equation approach then generates regular and singular hyperbolic waves, exponential localized structures, and Jacobi-elliptic periodic waves, together with their limiting bright, dark, and kink profiles.

The principal contribution is therefore the symmetry-compatible reduction, the explicit parameter constraints, and the unified orbit classification, rather than the auxiliary-equation procedure by itself. The graphical results illustrate exact shape-preserving translation but do not establish spectral stability, soliton radiation, optical-shock development, or a continuously evolving frequency shift. These effects require perturbation analysis or direct numerical propagation of the full equation and remain suitable topics for future investigation.

Disclosure. The authors claim there is no conflict of interest.

Funding and acknowledgment. The work of the last author (AB) was supported by Grambling State University through the Endowed Chair of Mathematics. The author gratefully acknowledges this support.

Authors contribution. Conceptualization: L.K. and A.B.; methodology and analytical investigation: L.K., A.H.A., M.A.S.M., and A.B.; validation and visualization: A.H.A. and M.A.S.M.; writing—original draft preparation: L.K. and A.H.A.; writing—review and editing: all authors; supervision: A.B. All authors have read and approved the final version of the manuscript.

References

1. Ala, V. (2022). New exact solutions of space-time fractional Schrödinger–Hirota equation. *Bulletin of the Karaganda University. Mathematics Series*, (3), 17–24.
2. Dai, C.-Q., & Zhang, J.-F. (2006). New solitons for the Hirota equation and generalized higher-order nonlinear Schrödinger equation with variable coefficients. *Journal of Physics A: Mathematical and General, 39*(4), 723–737.
3. Dowluru, R. K., & Bhima, P. R. (2011). Influences of third-order dispersion on linear birefringent optical soliton transmission systems. *Journal of Optics, 40*(3), 132–142.
4. 4. Du, Y., Yin, T., & Pang, J. (2024). The exact solutions of Schrödinger–Hirota equation based on the auxiliary equation method. *Optical and Quantum Electronics, 56*, 712.
5. Hasegawa, A., & Kodama, Y. (1995). *Solitons in optical communications*. Clarendon Press.
6. Jawad, A. J. M., & Abu-AlShaeer, M. J. (2023). Highly dispersive optical solitons with cubic law and cubic–quintic–septic law nonlinearities by two methods. *Al-Rafidain Journal of Engineering Sciences, 1*(1), 1–8.
7. Jihad, N., & Abd Almuhsan, M. A. (2023). Evaluation of impairment mitigations for optical fiber communications using dispersion compensation techniques. *Al-Rafidain Journal of Engineering Sciences, 1*(1), 81–92.
8. Kodama, Y., Romagnoli, M., Wabnitz, S., & Midrio, M. (1994). Role of third-order dispersion on soliton instabilities and interactions in optical fibers. *Optics Letters, 19*(3), 165–167.
9. Tian, G., & Meng, X. (2024). Exact solutions to fractional Schrödinger–Hirota equation using auxiliary equation method. *Axioms, 13*, 663.
10. Zhidkov, P. E. (2001). *Korteweg–de Vries and nonlinear Schrödinger equations: Qualitative theory* (Lecture Notes in Mathematics, Vol. 1756). Springer.
11. Ouahid, L., Abdou, M. A., Alshahrani, D. O., & Akgül, A. (2025). New periodic wave solution for time-fractional perturbed nonlinear Schrödinger equation arising in optical fiber via newly extended mapping scheme. *Optical Review, 32*, 608–618.
12. Trouba, N. T., Xu, H., Alngar, M. E. M., Shohib, R. M. A., El-Meligy, M., Zhu, X., & Sharaf, M. (2025). Optical soliton solutions of the stochastic generalized nonlinear Schrödinger equation with arbitrary refractive index in Itô sense. *Scientific Reports, 15*, 36172.
13. Afridi, M. I., Islam, T., Akbar, M. A., & Osman, M. S. (2024). The investigation of nonlinear time-fractional models in optical fibers and the impact analysis of fractional-order derivatives on solitary waves. *Fractal and Fractional, 8*(11), 627.
14. Olver, P. J. (1993). *Applications of Lie groups to differential equations* (2nd ed.). Springer.
15. Bluman, G. W., & Kumei, S. (1989). *Symmetries and differential equations*. Springer.

Kaur, L., Arnous, A.H., Murad, M.A.S., Biswas, A. (2026). Dispersive Optical Soliton Perturbation with Schrodinger-Hirota Equation by Lie Symmetry. *Ukrainian Journal of Physical Optics*, *27*(3), 03238 – 03258. doi: 10.3116/16091833/Ukr.J.Phys.Opt.2026.03238

Анотація. *У цьому дослідженні вивчаються розв'язки типу біжучої хвилі збуреного рівняння Шредінгера–Хіроти, яке враховує дисперсію третього порядку, нелінійну дисперсію, міжмодову дисперсію, самокрутизну імпульсу та самочастотний зсув. Комплексне рівняння зводиться до еквівалентної зв'язаної системи дійсних рівнянь, для якої визначаються точкові симетрії Лі. Сумісна лінійна комбінація генераторів трансляції та фазового обертання приводить до редукції типу біжучої хвилі, що задовольняє явний зв'язок між фазовою частотою та параметром симетрії. Для гілки з нульовою сталою інтегрування редуковане нелінійне звичайне диференціальне рівняння розв'язується методом узагальненого допоміжного рівняння. Отримано гіперболічні, експоненціальні та еліптичні розв'язки Якобі за відповідних умов невиродженості, дійсності та ненульового знаменника. Їхня гранична поведінка дає змогу розрізнити кінкові, темні, яскраві, сингулярні та нелокалізовані профілі. Діаграми інтенсивності ілюструють характерні морфології поширення, однак не використовуються як доказ стійкості.*

Ключові слова: *дисперсія, симетрія Лі, кноїдальні хвилі, рівняння Шредінгера-Хіроти, оптичні солітони*